Composite Structures 337 (2024) 118057

Contents lists available at ScienceDirect

Composite Structures

journal homepage: www.elsevier.com/locate/compstruct

# Fatigue behaviour of glass-fibre-reinforced polymers: Numerical and experimental characterisation

B. Alcayde [a,b], M. Merzkirch [c], A. Cornejo [b,a,*], S. Jiménez [a,b], E. Marklund [c], L.G. Barbu [a,b]

[a] Centre Internacional de Mètodes Numèrics en Enginyeria (CIMNE), Campus Norte UPC, 08034 Barcelona, Spain
[b] Universidad Politécnica de Cataluña (UPC), Campus Norte UPC, 08034 Barcelona, Spain
[c] Research Institutes of Sweden AB, Box 104, SE-431 22, Mölndal, Sweden

ARTICLE INFO

*Keywords:*
Composite material
High cycle fatigue
Serial–parallel rule of mixtures
Fracture mechanics
Finite element method

ABSTRACT

This work presents a novel numerical methodology to model the degradation and failure of composite materials like GFRP submitted to monotonic and high cycle fatigue loads. This is done by using the Serial–Parallel Rule of Mixtures homogenisation technique together with a proper mechanical characterisation of the constituent materials of the composite. This paper also proposes an efficient way of estimating the fatigue properties of each of the material constituents (fibre or matrix) to comply with the experimental results obtained at composite level; this enables to estimate the fatigue strength of any stacking/orientation of fibres with only one mechanical characterisation of the material properties. A comparison of the results obtained analytically and experimentally for GFRP is presented. The results show the applicability and accuracy of the proposed methodology in this field.

## 1. Introduction

Given the extensive application that composite materials have nowadays in different industries, due to their numerous advantages, the study of composite materials is a field that is rising in interest. One of the issues that stands out is the prediction of fatigue life in composite materials and, reviewing the literature, it can be noticed that research on this topic is, likewise, in a stage of growth and that it still has a long way to mature. The first methodologies used for the fatigue life prediction in composite materials are modifications of those developed in the 1960s and 1970s for metals under the assumption that composite materials do not suffer from fatigue. Nowadays, it is well known that the behaviour of composite materials under cyclic loads is very different from that of metals. While fatigue in metals has its origin in a crack that propagates until it completely breaks, in composite materials it is a much more complex process since there are various damage accumulation mechanisms and failure modes. Following the classification proposed by Sendeckyj [1], the damage models can be divided in three big groups: fatigue life models, phenomenological models and progressive damage models. A detailed summary can be found in [2].

Most of the literature published during the last decades is centred in the study of the damage that initiates between layers, *i.e.* delamination. This is, precisely, one of the most feared modes of damage in composite materials subjected to fatigue due to the great complexity that it entails. The most remarkable methods for its numerical study are the Virtual Crack Closure Technique (VCCT) [3,4], based on fracture mechanics, and the Cohesive Zone Model (CZM) [2,5–8], based on continuous damage mechanics. However, numerous authors highlight the need for further research in the development of approaches that allow a better prediction of crack formation. The most recent research are based on the combination of VCCT methods with Phase Field Model (PFM) [9–12] or the eXtended Finite Element Method (X-FEM) [3,13]. These combinations allow to implicitly account highly complex fracture patterns and to predict crack initiation, branching and merging [14,15]. Thus, despite the promising route to analyse crack initiation and propagation with considerable ease that these methodologies offer, the computational cost is high since there is a need of discretising with Finite Elements (FE) each layer of the composite. In this paper, a phenomenological homogenisation technique called Serial/Parallel Rule of Mixtures (SP-RoM) has been used to model the composite material mechanical behaviour. The main advantage of this model is its *generality* (different constitutive laws can be used for the matrix and fibre), *adaptability* (once the simple materials have been characterised, one can simulate different stacking sequences and orientations automatically) and *efficiency* (the SP-RoM homogenises the $n$ layers in the kinematically needed finite elements, avoiding the need of discretising each layer). Thus, it has been considered that the matrix behaves following an isotropic damage model while the fibre follows

* Correspondence to: Campus Norte UPC, 08034 Barcelona, Spain.
*E-mail address:* alejandro.cornejo.velazquez@upc.edu (A. Cornejo).

https://doi.org/10.1016/j.compstruct.2024.118057
Received 13 September 2023; Received in revised form 31 January 2024; Accepted 21 March 2024
Available online 30 March 2024

a High Cycle Fatigue (HCF) damage model. As will be detailed later, the isotropic damage model considers that the material degradation is developed in all directions alike and only depends on one scalar damage variable [16,17]. On the other hand, the HCF model establishes a relationship between the residual strength of the material and the evolution of the damage threshold, controlled by the internal variables of the material and by new variables of the fatigue state [18].

Another field of study linked to the prediction of fatigue life in composite materials is the development of *time-advance strategies* that allow to reduce the number of calculations and, therefore, the computational cost. The different proposed methodologies can be divided into four groups: Proper Orthogonal Decomposition (POD) [19], Proper Generalised Decomposition (PDG) [20], Large Time Increments (LATIN) [21] and cycle-jumps. POD is a linear procedure that makes a given collection of input data and creates an orthogonal basis constituted by functions estimated as the solutions of an integral eigenvalue problem decomposing a physical field depending on the different variables that that influence its physical behaviours. On the other hand, PGD is an iterative numerical method for solving boundary value problems (BVPs), that is, partial differential equations constrained by a set of boundary conditions, such as the Poisson's equation or the Laplace's equation. Unlike the two previous methodologies, LATIN represents a break with classical incremental methods in the sense that it is not built on the notion of small increments. It is an iterative method that sometimes starts with a relative gross approximation.

The cycle-jump strategies are based on detecting when some load stabilisation condition is reached and, in that case, omitting the calculation of a certain number of cycles. In Kiefer's thesis [22], a detailed comparison between four cycle-jump models can be found: Peerling's model [23], Turon model [2], Harper model [6] and Kawashita and Hallet model [24]. Some of the most recent studies are those proposed by Russo et al. [25], Sally et al. [26] and Magino et al. [27]. The Smart Cycle Strategy developed by Russo [25] provides a fast preliminary evaluation of the fatigue behaviour of composite structures based on the hypothesis that the stress redistribution can be neglected until a damage in the fibre and/or matrix at an element/layer level is verified. The kinetic damage rate model proposed in Sally et al. [26] predicts the damage evolution in composite materials during fatigue and spectral loadings. The model presented more recently by Magino [27] is based on the parametrisation of the loading curve which enables to reformulate the model in terms of a cycle-scale and a logarithmic cycle-scale variable, respectively. In this paper, a different version of the last one will be used [18,28] since it allows to efficiently predict the initiation and propagation of the damage on the model while loads are applied, independently of their typology.

Therefore, the main objective of the undergone research has been to propose a generalisation of the SP-RoM technique to improve the accuracy of crack initiation and propagation modelling in GFRP materials subjected to fatigue loading, since it is one of the phenomena of most common failure. In addition, the HCF constitutive law with a time-advance strategy has not yet been validated for composite materials in combination with the SP-RoM and, therefore, it is intended to review and expand it. On the other hand, a generalised method that allows calibrating the fatigue parameters of the component materials, fibre and matrix, from the data at composite level has been proposed.

The paper is organised in several sections, starting with Section 2, which describes the methodology that has been followed to reproduce the different models that govern the behaviour of composite materials, such as damage, plasticity, and HCF. The model used to simulate the composite material, SP-RoM, and the method to systematically calibrate its material constituents are described in Section 3. The setup of the experimental tests developed by RISE are detailed in Section 4. To validate the correct operation of this method, some application cases are presented in Section 5 in which the results obtained numerically are compared with the experimental data. Finally, the conclusions are presented in Section 6.

## 2. Component constitutive model

This section describes the constitutive models used in each of the component materials of the composite materials analysed, *i.e.*, the fibre and matrix materials. Once the constitutive laws governing the mechanical behaviour of simple materials are known, it is necessary to present the SP-RoM homogenisation theory [29–33], which allows us to obtain the behaviour of the composite material from the participations, orientations and individual constitutive behaviour of the fibre and matrix in it.

### 2.1. Isotropic damage model

According to experimental evidence, the matrix does not get damaged due to fatigue, instead it suffers from monotonic-type degradation [34–37]. This is because, in the experiments carried out, the loading of the first cycle itself induces cracks in the matrix, since it has a very low yield strength compared to that of the fibre. Therefore, the isotropic damage model has been used to reproduce the behaviour of the matrix. This model is widely known and only some brief explanations will be given from here on. The readers can find the complete description in [16,17].

For the isotropic damage model, the material degradation is developed in all directions alike and only depends on one scalar damage variable $d$, which ranges from 0 (intact) to 1 (fully damaged); Hence, the isotropic damage constitutive law reads

$$\boldsymbol{\sigma} = (1-d)\,\mathbf{C}_0\,\boldsymbol{\varepsilon} = (1-d)\,\boldsymbol{\sigma}_0, \tag{1}$$

where $d$ is the internal damage variable, $\boldsymbol{\varepsilon}$ is the strain tensor (assuming small strains), $\mathbf{C}_0$ is the undamaged constitutive tensor, $\boldsymbol{\sigma}$ is the Cauchy's stress tensor and $\boldsymbol{\sigma}_0$ is the effective Cauchy's stress tensor measured in the *"non-damaged"* space.

In order to know if the material is in elastic or non linear regime, a yield surface has to be defined such as

$$\Phi = f(\boldsymbol{\sigma}_0) - \kappa \leq 0 \tag{2}$$

where $f(\boldsymbol{\sigma}_0)$ is the so-called equivalent effective stress whose definition depends on the yield surface of interest (Rankine, Simo-Ju, Drucker–Prager, etc.), and $\kappa$ is the stress threshold (related to the material strength), which each yield surface will define and updated afterwards. In this paper, a Von Mises yield surface has been chosen for the matrix, thus:

$$f(\boldsymbol{\sigma}_0) = \sqrt{3J_2} \tag{3}$$

being $J_2$ the second invariant of the deviatoric stress tensor. By using this yield surface, the material strength threshold $\kappa$ is a historical value that must be updated at each time step according to

$$\kappa = \max(\kappa_0\,,\, \max(f(\boldsymbol{\sigma}_0)_{t\in[0,t_n]})) \tag{4}$$

where $\kappa_0$ is the initial threshold (yield stress in tension) and $f(\boldsymbol{\sigma}_0)_{t\in[0,t_n]}$ the maximum uniaxial stress achieved up to the current solution step $t_n$. A complete description of the different yield surfaces can be found in [16,38–40]. The implemented damage model in Kratos-Multiphysics [41] offers different damage evolution laws like: linear softening, exponential softening, stress/strain curve defined by points, among others. When Eq. (2) is not satisfied, an updated damage $d$ must be calculated according to (assuming exponential softening) [17,42]:

$$d = 1 - \frac{\kappa_0}{f(\boldsymbol{\sigma}_0)} \cdot exp\left[A \cdot \left(1 - \frac{f(\boldsymbol{\sigma}_0)}{\kappa_0}\right)\right] \tag{5}$$

with

$$A = \left(\frac{g_f \cdot E}{\kappa_0^2} - \frac{1}{2}\right)^{-1} \geq 0 \tag{6}$$

where $E$ is the Young's modulus and $g_f$ the volumetric fracture energy. A high value of $g_f$ will induce a perfectly flat post-peak evolution.

### 2.2. High cycle fatigue model

As previously mentioned, supported by the experiments, it has been considered that the fibre is submitted to a high cycle fatigue behaviour. The HCF methodology employed in this paper is based on the work presented in Barbu [18] which was initially developed by Oller et al. [40]. More recently, other authors have worked in the direction of reducing the computational cost of this methodology [28] or generalising its use to other type of materials.

This constitutive law can be seen as a modified continuum damage model for mechanical fatigue analysis that is coupled with a cycle advance strategy for cyclic loading. The model establishes a relationship between the residual strength of the material and the evolution of the damage threshold, controlled by the internal variables of the material and by new variables of the fatigue state. In this model, it is assumed that the coalescence of micro-scale defects occurs during the cyclical loading period, which is reflected as a continuum reduction in the strength of the material, which occurs even in the elastic stage. Furthermore, it considers that stiffness degradation occurs only in the post-critical stage. The damage and the material threshold historical parameters of the model have a phenomenological meaning that indicates the irreversibility of the fatigue process.

The HCF constitutive law presented in [40] is an extension of the isotropic damage model proposed by Oliver et al. [17] briefly described in the previous Section. The constitutive law used in HCF is identical to the one defined for isotropic damage in Eq. (1). However, to account for the material degradation due to the cycling process, a new *fatigue reduction factor* $f_{red}$ is introduced in the yield condition as

$$\Phi(\boldsymbol{\sigma}_0) = \frac{f(\boldsymbol{\sigma}_0)}{f_{red}(N_c, R, S_{max})} - \kappa \leq 0 \tag{7}$$

where $f_{red}$ ranges from 1 (no fatigue) to 0 (maximum amplification due to fatigue). This parameter takes into account the effect of the acting cyclic load and, consequently, amplifies the stress state depending on the number of cycles applied, $N_c$, the reversion factor, $R = S_{min}/S_{max}$, and the maximum stress generated by the applied load, $S_{max}$. The number of cycles, $N_c$, along the simulation is updated based on the evolution of the equivalent stresses at the integration point level, *i.e.*, when maximum and minimum values of the stress are detected this indicates that a new cycle has overcome. Therefore, $S_{max}$, $S_{min}$ and $R$ variables are updated at each new cycle, if necessary. The calculation of damage $d$ and the historical stress threshold $\kappa$ update is done analogously to the isotropic damage case with a nuace: $d = d\left(\frac{f(\sigma_0)}{f_{red}}\right)$ by using Eq. (5).

The following function is proposed to describe the variation of the residual strength [18,28]:

$$f_{red} = e^{-B_0 \cdot (log_{10} N_c)^{\beta_f^2}} \tag{8}$$

where $B_0$ is obtained as a function of the ratio $S_{max}/S_u$:

$$B_0 = -\left(\frac{ln(S_{max}/S_u)}{(log_{10} N_f)^{\beta_f^2}}\right) \tag{9}$$

and the number of cycles to failure $N_f$, by:

$$N_f\left(S_{max},\ R\right) = 10^{\left[\left[-\frac{1}{\alpha_t(R)} \ln\left(\frac{S_{max}-S_{th}(R)}{S_u-S_{th}(R)}\right)\right]^{\frac{1}{\beta_f}}\right]} \tag{10}$$

in which $\alpha_t$ and $\beta_f$ are material parameters that need to be adjusted according to experimental tests. The description of these parameters can be found in [28]. An S–N (Stress versus Number of cycles) curve can be seen as a material property that relates the maximum stress achieved during the cyclic load and the amount of cycles that the sample withstands up to failure. Since the minimum stress can be different depending on the load, several S–N curves are estimated experimentally according to the $R$ factor. The S–N curve is sufficient to determine the fatigue life when $S_{max}$ and $R$ remain constant. However, when dealing with different load interactions the main focus resides on the residual strength curve. The curve quantifies the loss of strength in the material as the number of cycles accumulates and as load characteristics change. In Eqs. (9) and (10), $S_{min}$ is the minimum stress, $S_u$ is the ultimate stress, $S_e$ is the endurance limit for any given reversion factor and $S_{th}$ is the elastic threshold limit.

As mentioned by Barbu [18], fatigue models are usually limited to correctly describing the S–N curves and, based on the level of stress applied, estimate the fatigue life. When the $N_c$ corresponding to the Wöhler curve has been reached for a certain level of stress, the respective Gauss point has suffered complete degradation. However, this model utilises the respective $N_c = N_f$ point as the starting point for damage accumulation and the nonlinear zone, for that particular Gauss point. That mirrors the initiation point for a micro-crack. Posterior damage accumulation is an indicator of a rearrangement of the internal structure of the material followed by micro-fisuration and a completely degraded Gauss point ($d_{GP} = 1$) represents the formation of a macro-crack in the volume associated to the integration point. At macro-scale level, a tracking of the damage propagation throughout the continuum is an indicator of a crack propagation and total structural fracture is considered to have occurred when the crack has propagated through the entire cross-sectional area.

### 2.3. Time advancing strategy

The fatigue degradation analysis is done with several steps by cycle, which is very computationally expensive. To overcome this issue, load advancing strategies have been developed. As previously mentioned, Barbu [18] presented a step wise load-advancing strategy for cyclic loading that yields convergence in reasonable computational time for highly nonlinear behaviour occurring past the S–N curve. The algorithm is also effective when dealing with combinations of cyclic loads.

The proposed strategy uses the formulation described in Oller et al. [40] and is divided into two phases: load-tracking phase and large increments phase. The first one is defined by load-advance being conducted by small time increments, with the consequent load variation following a cyclic path. The second phase is characterised by load-advance being done with large increments of number of cycles. Unlike the formulation proposed by Oller, the strategy presented in Barbu [18] automatically switches from one phase to the other, going repeatedly back and forth between both in accordance with the loading input and the damage increase rate. The strategy was developed for metals and in [18,28] applied for long fibre reinforced composites. A detailed description of the algorithms can be found in the Appendix, summarising how the time advancing strategy and the SP-RoM are combined.

## 3. Constitutive modelling of GFRP with the serial–parallel rule of mixtures

### 3.1. Serial–parallel rule of mixtures law

In the previous section, a detailed description of the constitutive models for each of the material components, *i.e.* the matrix and the fibre, have been given. Next, since the two material components are interacting within the GFRP composite type material, a homogenisation technique is needed in order to phenomenologically estimate the mechanical properties of the bulk composite material. In this regard, the Serial–Parallel Rule of Mixtures (SP-RoM) has been used [28].

The SP-RoM can be defined as a phenomenological homogenisation, in which the behaviour of the composite material is obtained from the constitutive response of its component materials. Through this, it is possible to take into account the non-linear behaviour of the composite without requiring the enormous computational cost. This theory was

developed by Rastellini et al. [43,44] and is an evolution of the theory of parallel mixtures developed by Car [45]. A detailed description of the SP-RoM algorithm and many examples of its application can be found in [29–33].

The main hypotheses for the numerical formulation are summarised in

1. The composite is formed by only two components: fibre and matrix.
2. Component materials have the same strain in parallel (fibre) direction.
3. Component materials have the same stress in serial direction.
4. Composite material response is in direct relation with the volume fractions of compounding materials.
5. Homogeneous distribution of phases is considered in the composite.
6. Perfect bonding between components is considered; this condition can be alleviated by using low values of the shear modulus in one of the material components together with an orthotropic behaviour.

As this formulation proposes to combine the behaviour of the component materials in order to obtain the response of the composite material, the global anisotropy of composite material is considered as the result of the interaction of the components. Additionally, the SP-RoM theory allows component materials that present any type of non-linearity such as damage and plasticity to be analysed.

The strain tensor $\boldsymbol{\varepsilon}$ is decomposed into a serial part $\boldsymbol{\varepsilon}_s$ and a parallel part $\boldsymbol{\varepsilon}_s$ by means of the projection tensors ($\mathbf{P}_P$, $\mathbf{P}_S$) of fourth order in parallel and in serial directions, respectively:

$$\boldsymbol{\varepsilon} = \boldsymbol{\varepsilon}_P + \boldsymbol{\varepsilon}_S \tag{11}$$

$$\boldsymbol{\varepsilon}_P = \mathbf{P}_P : \boldsymbol{\varepsilon} \qquad \boldsymbol{\varepsilon}_S = \mathbf{P}_S : \boldsymbol{\varepsilon} \tag{12}$$

The stress tensor $\boldsymbol{\sigma}$ is also separated into its serial components $\boldsymbol{\sigma}_S$ and its parallel components $\boldsymbol{\sigma}_P$:

$$\boldsymbol{\sigma} = \boldsymbol{\sigma}_P + \boldsymbol{\sigma}_S \tag{13}$$

$$\boldsymbol{\sigma}_P = \mathbf{P}_P : \boldsymbol{\sigma} \qquad \boldsymbol{\sigma}_S = \mathbf{P}_S : \boldsymbol{\sigma} \tag{14}$$

where the fourth-order projection tensors are found through the second-order parallel projection tensor $\mathbf{N}_P$ and the fourth-order identity tensor $\mathbf{I}$,

$$\mathbf{P}_P = \mathbf{N}_P \otimes \mathbf{N}_P \tag{15}$$

$$\mathbf{P}_S = \mathbf{I} - \mathbf{P}_P \tag{16}$$

$\mathbf{N}_P$ is a function of the unit vector $\mathbf{e}_1$ that indicates the direction of the behaviour in parallel, that is, the direction of the fibre

$$\mathbf{N}_P = \mathbf{e}_1 \otimes \mathbf{e}_1 \tag{17}$$

*Equilibrium and compatibility equations in the composite layers*

In order to minimise the computational cost, the numerical implementation of the SP-RoM was developed to decompose the composite $c$ into a certain number of layers $n_{lay}$, such that each layer $j$ is made up of a matrix $m$ and a fibre $f$ mixture. Consequently, according to the enunciated hypotheses, the following equilibrium and deformation compatibility equations must be fulfilled in each layer of the composite:

*Parallel behaviour*

$${}^{c}_{j}\boldsymbol{\varepsilon}_P = {}^{m}_{j}\boldsymbol{\varepsilon}_P = {}^{f}_{j}\boldsymbol{\varepsilon}_P \tag{18}$$

$${}^{c}_{j}\boldsymbol{\sigma}_P = {}^{m}_{j}k \cdot {}^{m}_{j}\boldsymbol{\sigma}_P + {}^{f}_{j}k \cdot {}^{f}_{j}\boldsymbol{\sigma}_P \tag{19}$$

*Serial behaviour*

$${}^{c}_{j}\boldsymbol{\sigma}_S = {}^{m}_{j}\boldsymbol{\sigma}_S = {}^{f}_{j}\boldsymbol{\sigma}_S \tag{20}$$

$${}^{c}_{j}\boldsymbol{\varepsilon}_S = {}^{m}_{j}k \cdot {}^{m}_{j}\boldsymbol{\varepsilon}_S + {}^{f}_{j}k \cdot {}^{f}_{j}\boldsymbol{\varepsilon}_S \tag{21}$$

where $k$ is the volumetric fraction of each matrix and fibre component. The system of equations described in Eqs. (18) and (21) must be solved simultaneously at each integration point of the structure. Since this system of equations is implicit, an iterative solution algorithm (Newton–Raphson type) is used [28,29,43,44].

### 3.2. Component characterisation

Testing the fibre and the matrix separately in the laboratory is a difficult task. For that reason, the complete composite is usually tested providing homogenised data. However, in order to simulate the behaviour of the laminate numerically with this formulation, it is necessary to know the properties of the individual component materials. This information is often not available and, for this reason, the method described below is proposed to characterise them without the need of testing them in the laboratory.

In this paper, supported by experimental evidence, it is considered that the fibre is the component that fails due to fatigue. Therefore, the method allows to transform data from fatigue at the composite level to a characterisation at the fibre level. The same method could be applied to the matrix if needed.

The SP-RoM technique allows obtaining a factor, $C$, that relates the stresses in the composite, $\sigma_c$ with the ones in the fibre (or matrix) at a any desired orientation (0°, 45°, 90°), $\sigma_f$. By means of this factor, one can transform the S–N curve at composite level (experimental input) to component level and, in this way, being able to characterise the fatigue behaviour of each material constituent (fibre in this case). As shown in Fig. 1, the same S–N curve of the fibre is obtained for different laminate sequences.

$$C = \frac{\sigma_f}{\sigma_c} \tag{22}$$

Once the S–N curve of the fibre has been determined, it is possible to obtain its fatigue parameters through a parameter optimisation code that includes the equations described in Section 2. Since the code requires S–N curve data for two different values of $R$, the Gerber formula (23), can be used to transform the data from $R = 0.1$ to $R = -1$. $S_a$, $S_u$ and $R$ in the equation correspond to the amplitude and ultimate stresses and the reversion factor, respectively.

$$S_a(R=1) = S_{max}(R=-1) = \frac{\left(\frac{1-R^R}{2} S_{max}(R^R)\right)}{1 - \left(\frac{\frac{1+R^R}{2} S_{max}(R^R)}{S_{ult}}\right)^2} \tag{23}$$

The previous equation is only valid for stress values close to $S_e$. Therefore, it is necessary to make a selection and adjust them.

In this paper, the homogenised data of the composite material have been obtained from experimentally testing two different stacking sequences in the laboratory, in the case of this study, 0/90 and 0/90/45. Considering both sequences allows validating the correct functioning of the methodology by comparing the obtained results with the experimental evidence. From the received homogenised composite data it has been possible to obtain its S–N curve and, afterwards, by means of transforming it, the one of the fibre. Thus, once the fibre has been characterised, the data can be used for any stacking sequence.

## 4. Experimental setup

### 4.1. Materials and specimen geometry

In this Section, a description of the manufacturing of the composite specimens is provided. Two laminates with two different layups,

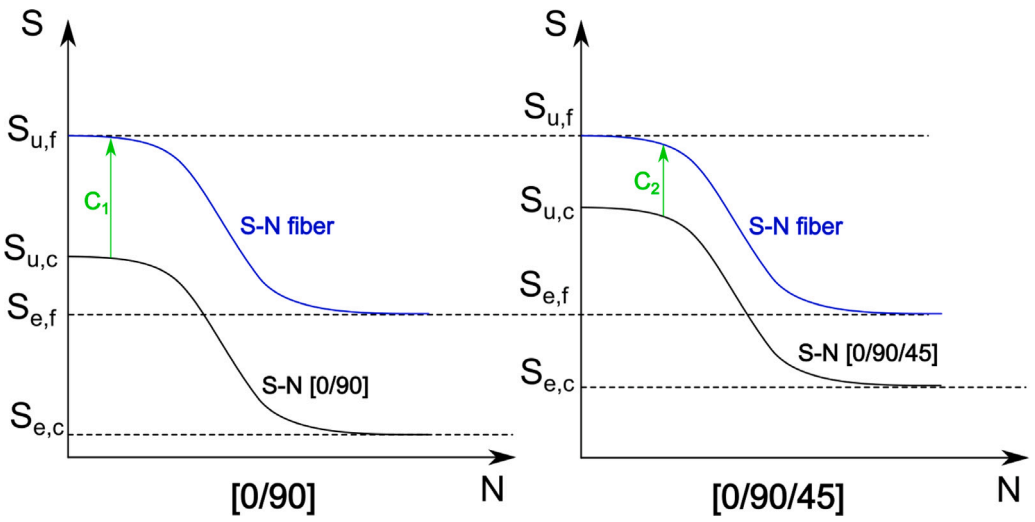


**Fig. 1.** Diagrams of the fibre S–N curve obtained from different composite stacking sequences.

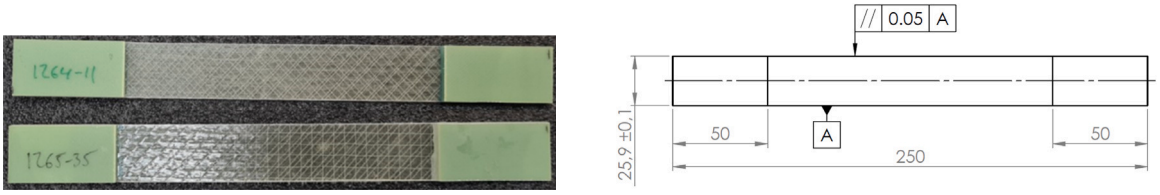


(a) (b)

**Fig. 2.** (a) Tabbed specimens ([0/90] top, [0/90/±45] bottom); b) Specimen geometry in accordance with ASTM D3039 ($L_0$ = 50 mm). The dimensions are expressed in mm.

*i.e.* $[0/90]_{2s}$([0/90/0/90/90/0/90/0]) and $[0/90/\pm 45]_s$ ([0/90/+45/-45/-45/+45/90/0]), have been manufactured via vacuum injection (in 0° direction at 0.114 Bar). Huntsman Araldite LY1564 resin and Aradur 22962 hardener (at a ratio 4:1) at room temperature are used and cured (reaching 0.31 Bar) at 80 °C for one hour and 150 °C for two hours. Overall, 4 layers of glass fibre EBX400 (bidirectional ±45° layup by Selcom srl with a surface weight of 408 g/m$^2$ with stitch yarns in the horizontal direction have been stacked up to a resulting thickness of the plates of approx. 1.4 mm and a size of approx. 630 × 630 mm.

The geometry of the specimens was chosen to be identical for both layups and tensile and fatigue testing. Composite tabs at both ends are used to avoid failure in the grips during the tests. The tabs are made of ±45° fibreglass in an epoxy resin, "G11" with a thickness of approximately 1.5 mm. Commercially available acrylic adhesive was used and cured at room temperature. Finally, the tabbed plates were water jet cut. The geometric details of the specimens with an aspect ratio ($L/w$ = 5.8) are given in Fig. 2. For further details on the investigation of the optical damage monitoring, and results on quasi-static and fatigue testing, see [46].

### 4.2. Monotonic test

The quasi-static tensile and fatigue tests were executed on an Instron servo-hydraulic testing machine with a maximum load capacity of 100 kN. The loading has been induced by the actuator located at the bottom of the test frame. The specimens were rigidly hydraulically gripped using diamond jaw surfaces and a pressure of 100 Bar. The specimens have been aligned with specimen stops on one side of each grip. The strain was measured with an extensometer (Instron) with a length of $L_0$ = 50 mm attached on the (thin) side of the specimen using rubber bands, see Figs. 3(a) and 3(b).

The displacement-controlled tensile tests were conducted at a nominal rate of 0.00011 1/s (1 mm/min for $L$ = 150 mm). The data acquisition rate was set to 20 Hz. Two specimens were tested for each layup.

### 4.3. Fatigue test

For the fatigue tests, the same specimen geometry and testing setup was used as for the tensile tests. The force-controlled fatigue tests were conducted at a stress ratio of $R$ = 0.1 (tension–tension fatigue) and a sinusoidal loading frequency of 5 Hz. Due to the low thickness of the specimens, and the likelihood of buckling, the stress ratio $R = -1$ has not been investigated, which would require shorter specimens which in turn would affect the fatigue lifetime. Two specimens per load level were tested for each layup. The data acquisition rate was set to 1000 Hz, resulting in 200 data points per cycle with a duration of 0.2 s.

Before the testing, the load string stiffness for each type of layup has to be determined aiming for proper test control. The maximum number of cycles till the test end (run out) was chosen to be $10^6$ cycles. Three load levels have been chosen with two tests each for each layup. Due to small differences in thickness of the manufactured samples, different maximum stresses are obtained. A total of 12 samples were tested to fatigue, whose results can be seen in Table 1.

## 5. Validation cases

The previous proposed methodology has been applied to simulate two different sequences of GFRP laminates. The specimens have been tested in the laboratory under monotonic and fatigue regimes and after, these tests have been reproduced numerically. In this section, a comparison between the experimental and numerical results is presented in order to validate the correct functioning of the methodology. The cases described in this work have been solved using the software Kratos-Multiphysics [41,47].

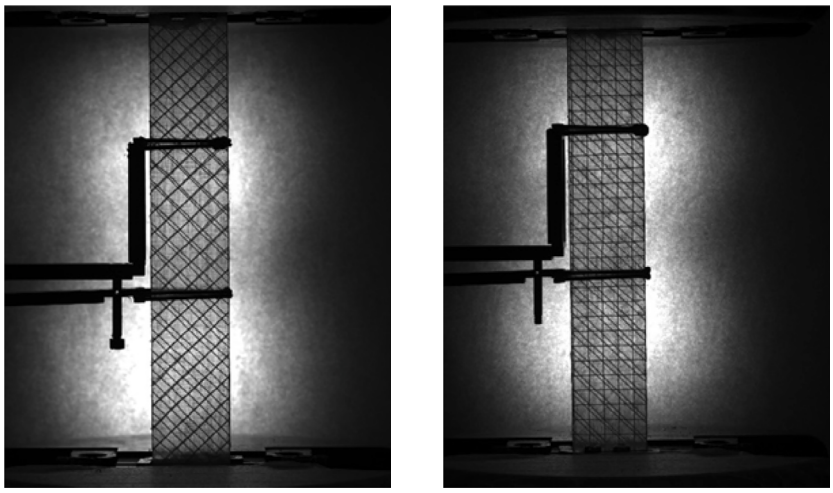

(a) (b)

**Fig. 3.** (a) Testing setup (tensile and fatigue) and clamped specimen with attached extensometer and backlight, (b) Field of View of the camera for qualitative detection ($[0/90]_{2s}$ layup with stitching yarns ±45° shown) (c) Field of View of the camera for qualitative detection ($[0/90/\pm 45]_{s}$ layup with stitching yarns 0°/90°/45° shown)

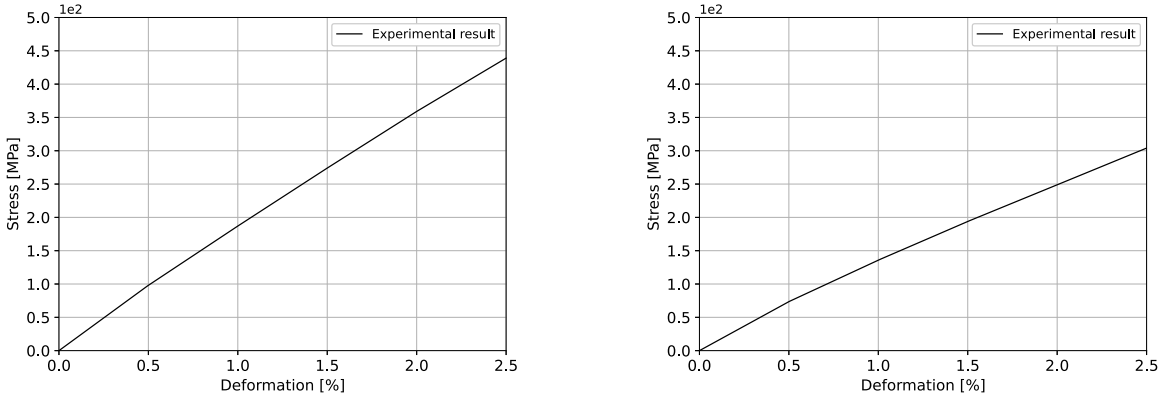


(a) (b)

**Fig. 4.** Stress-Strain (composite level) experimental results from the monotonic test for GFRP with stacking sequences 0/90 and 0/90/45.

**Table 1**
Experimental data for sequences 0/90 and 0/90/45.

| 0/90 | | 0/90/45 | |
|---|---|---|---|
| Number of cycles | Max stress [MPa] | Number of cycles | Max stress [MPa] |
| 1 | 449.1 | 1 | 335.2 |
| 1 | 442.6 | 1 | 301.4 |
| 69 | 424.6 | 69 | 296.9 |
| 94 | 407.7 | 174 | 293.9 |
| 1784 | 326.3 | 675 | 232.4 |
| 1596 | 317.9 | 2717 | 224.9 |
| 33944 | 232.3 | 13323 | 161.2 |
| 21371 | 226.1 | 18957 | 163.8 |

The data received from the laboratory (see Table 1 and Fig. 4) in monotonic and fatigue regime corresponds to the composite level; for this reason it has been necessary to establish a generalised methodology to extract the data from the composite to its individual component materials. As it can be noticed in Table 1, there are two stress values for the same number of cycles. This difference is a result of material fluctuations in the manufactured samples.

### 5.1. Monotonic test

The monotonic material properties of the fibre and the matrix have been characterised from the homogenised composite level data received from the laboratory tests following the methodology proposed in the previous section. The estimated material properties for the matrix and fibre are given in Table 3. Since the behaviour of the matrix is determined by the stress and strain points of the curve, its fracture energy has not been considered. On the other hand, as the fibre behaviour is on the domain previous to the softening, a tentative high level of fracture energy has been chosen. Two numerical simulations have been carried out for two different stacking sequences (0/90 and 0/90/45/-45) to verify the correct functioning of the methodology (see Table 2). It is important to note that the calibration of the individual components is done once, then the SP-RoM is able to compose the behaviour to model any stacking sequence and orientation. Fig. 5 shows a comparison of the results obtained numerically and in the experiment. As can be seen, the initial stiffness of the composite is consistently reproduced in both stackings as well as the post-yield regime. The experimental result obtained ends when reaching a 3% strain in which a sudden drop due to the fibre failure is expected.

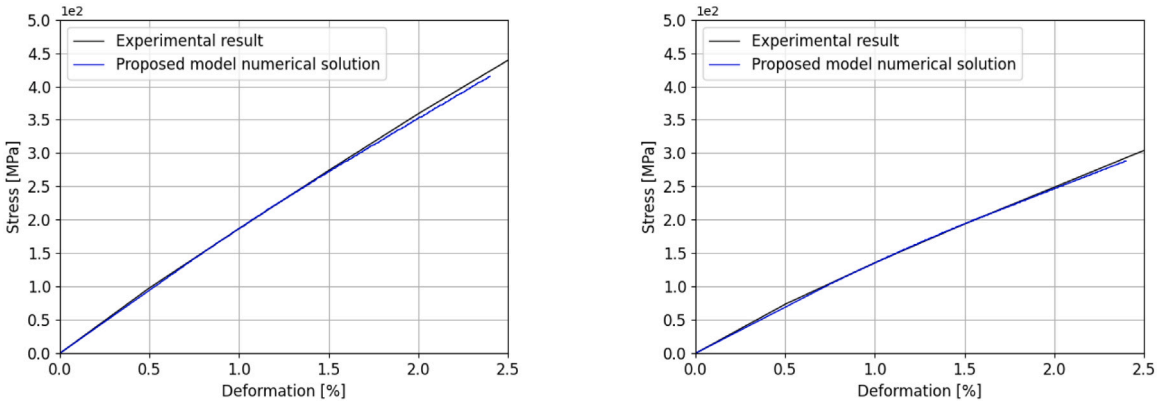


**Fig. 5.** Comparison of the results obtained numerically reproducing the monotonic test for the 0/90 and 0/90/45 sequences by considering the homogenised data and the component data with the SP-RoM model.

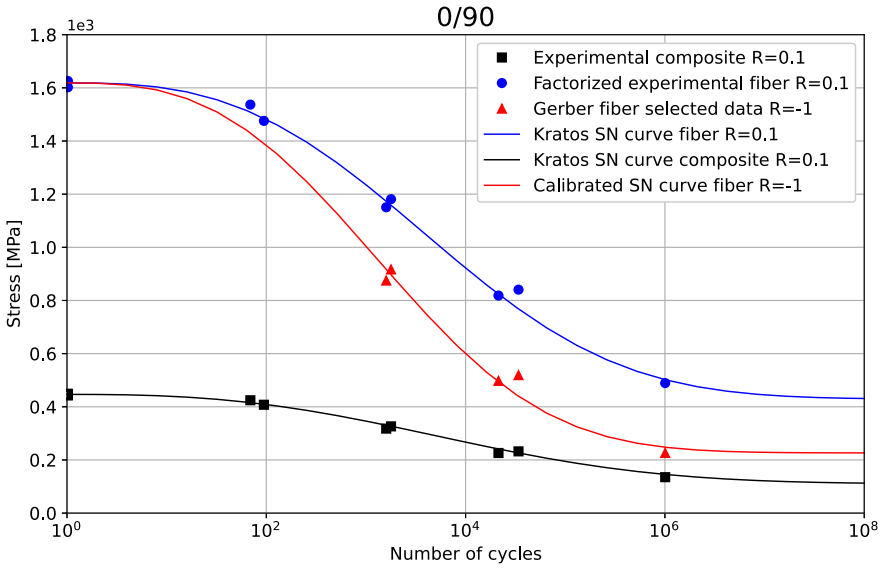


**Fig. 6.** Experimental and numerical data of the composite with sequence 0/90 for $R = 0.1$ and $R = -1$.

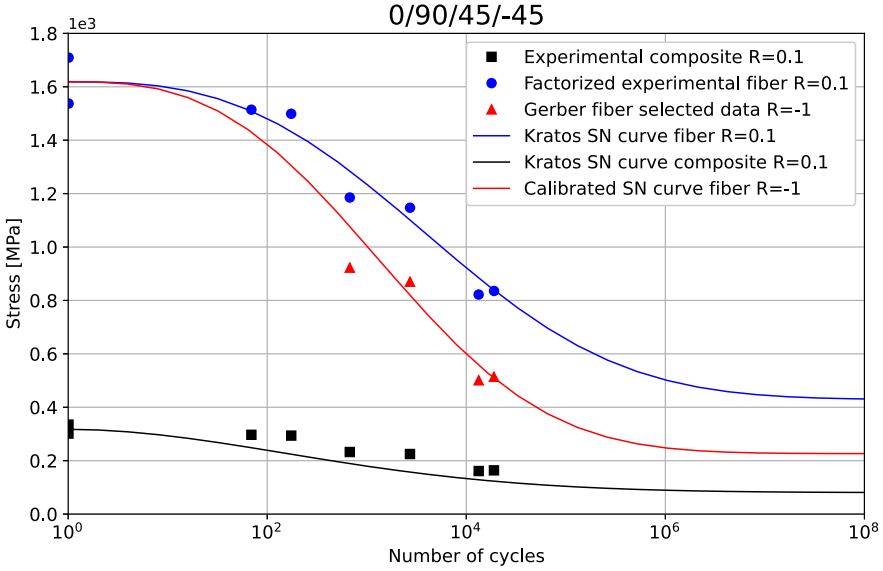


**Fig. 7.** Experimental and numerical data of the composite with sequence 0/90/45 for $R = 0.1$ and $R = -1$.

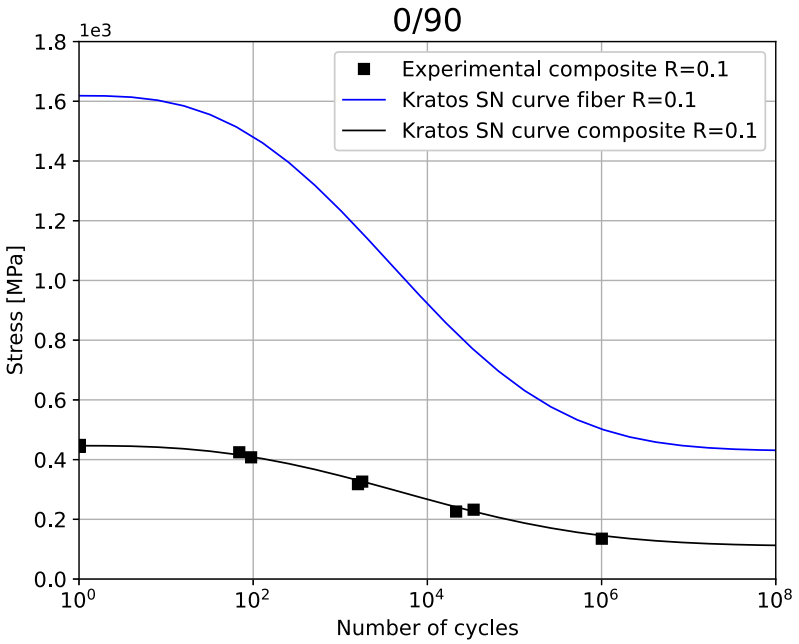


**Fig. 8.** Fibre and composite curves numerically obtained from the composite homogenised data for the sequence 0/90.

**Table 2**
Composite materials definition for each layer of the specimens for 0/90 and 0/90/45 sequences.

| Layer Id | Layer volumetric participation [%] | Euler angles [$\phi$, $\theta$, $\psi$] [Deg] |
|---|---|---|
| 1 | 0.25 | [0,0,0] |
| 2 | 0.25 | [90,0,0] |
| 3 | 0.25 | [45,0,0] |
| 4 | 0.25 | [−45,0,0] |

**Table 3**
Monotonic fibre and matrix properties.

| | MATRIX | FIBER |
|---|---|---|
| Volumetric Participation [%] | 0.55 | 0.45 |
| Young Modulus [MPa] | 2580 | 68 800 |
| Yield stress [MPa] | 340 | 1199 |
| Stress Curve Points [MPa] | [340, 370, 403, 436, 454, 472] | – |
| Strain Curve Points [%] | [1.34, 1.50, 1.75, 2.00, 2.25, 2.50] | – |
| Fracture Energy [J/m$^2$] | – | $10^5$ |

### 5.2. High cycle fatigue test

Following the methodology previously described, the fatigue parameters of the fibre have been characterised from the homogenised experimental data of the composite submitted to fatigue for $R = 0.1$ (Table 4). These parameters will be used to obtain the S–N curve. The input data obtained using the Gerber parabola for the fibre and composite and their output S–N curves are summarised in Figs. 6 and 7. Figs. 8 and 9 show that the fibre S–N curve numerically obtained for both sequences of the composite coincide, which is an expected outcome.

Figs. 6 and 7 show the process followed to calibrate the fatigue parameters of the fibre. The experimental points of the composite for $R = 0.1$ have been factorised by using the ratio $C$, that relates the fibre and composite stresses, to obtain the points of the S–N curve of the fibre for $R = 0.1$. Afterwards, the points for $R = -1$ have been calculated by means of the Gerber formula (Eq. (23)). Finally, the fatigue parameters of the fibre have been determined through the parameter optimisation code mentioned in Section 2.

In order to check the correct functioning of the proposed methodology, the stresses in the different orientations of the fibres have been monitored. For that, the code has been extended to be able to get information from the different layers of the composite. As shown in Figs. 10 and 11, the fibres oriented at 0° are withstanding larger stresses in both sequences. In the 0/90 sequence, the layer with 90° oriented fibres supports very low stresses while in the case of the 0/90/45 sequence it is distributed with the layers with 45° oriented fibres. Although layers oriented at 45° and -45° seem to withstand the same stress of layer oriented at 90°, the stress is very similar since it is considered in the $x$-direction.

**Table 4**
Fibre fatigue parameters.

| $\frac{S_e}{S_u}$ | $S_{th,R_1}$ | $\alpha_f$ | $\beta_f$ | $AUX_{R_1}$ |
|---|---|---|---|---|
| 0.139 | 3.224 | 0.026 | 2.843 | −0.015 |

The fatigue test has been reproduced applying the time-advance strategy. The different load scenarios considered in the simulations are summarised in Table 5. The numerical S–N curve obtained by considering the maximum stress for each load scenario shows good agreement with the experimental data (Fig. 12 and Fig. 13). The five numerical values obtained have been compared with the eight experimental values received from the laboratory only considering the HCF region.

Figs. 14 to 17 illustrate the advance in time strategy for load scenarios 1 and 5 for both studied sequences. For the 0/90 sequence in the load scenario 1, the time-advance strategy performs a jump of 1008 cycles, which corresponds to a stress in the fibre of 1234 MPa (Figs. 14 and 15). In Fig. 10 it can be seen that it is the maximum stress that the layer of fibres oriented at 0° withstands. The same thing happened in the case of the 0/90/45 sequence, which performs a jump of 970 cycles (see Fig. 15) since, by distributing the stresses between the layers with fibres oriented 90°, 45° and -45°, the layer with fibres oriented at 0° continues to be the one that supports the greatest stresses (see Fig. 11). On the other hand, from the point of view of the composite, the jump corresponds to 320.2 MPa and 225.65 MPa for the 0/90 and 0/90/45 sequences, respectively. These values coincide with the ultimate stress, $S_u$, of the composite for these sequences.

As shown in Figs. 16 and 17, in the load scenario 5, the jump performed by the advance strategy in both the case of the composite

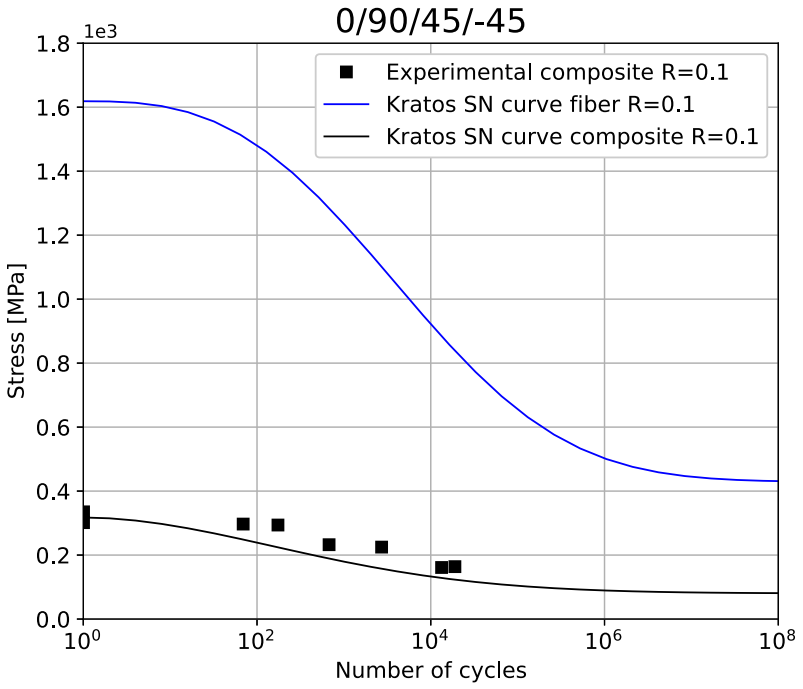


**Fig. 9.** Fibre and composite curves numerically obtained from the composite homogenised data for the sequence 0/90/45.

**Table 5**
Load scenarios and numerical results in fatigue life.

| LOAD | Max Displ [mm] | 0/90 | | 0/90/45/−45 | |
|---|---|---|---|---|---|
| | | Max stress [MPa] | Number of cycles | Max stress [MPa] | Number of cycles |
| 1 | 4.50 | 320.20 | 1008 | 225.65 | 970 |
| 2 | 4.00 | 288.20 | 1397 | 204.62 | 2709 |
| 3 | 3.50 | 255.80 | 3770 | 182.90 | 7341 |
| 4 | 3.25 | 238.90 | 6287 | 171.48 | 12 250 |
| 5 | 3.00 | 221.90 | 21 478 | 159.87 | 20 943 |

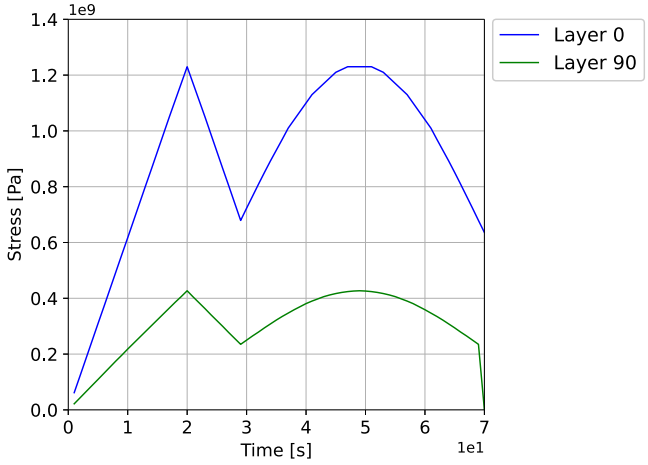


**Fig. 10.** Tracking of the stresses in the different layers of the composite for the sequence 0/90.

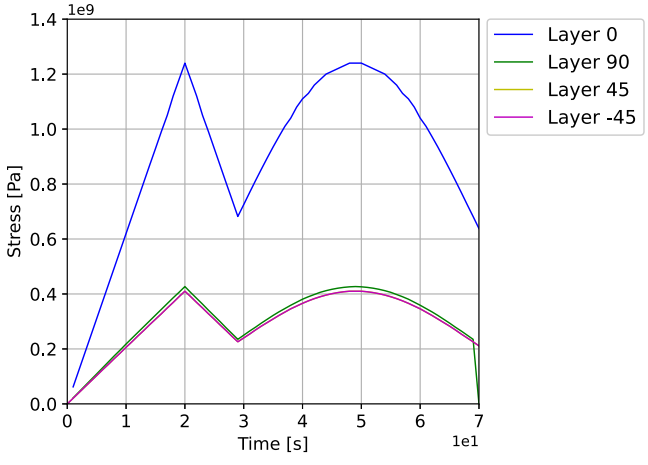


**Fig. 11.** Tracking of the stresses in the different layers of the composite for the sequence 0/90/45.

and the fibre is in accordance with that stress value. The maximum stress reached in the fibre is 823 MPa.

## 6. Conclusions

In this paper, a generalised methodology for the numerical analysis of high cycle fatigue in composite materials has been proposed. This method couples the time-advance strategy for high cycle fatigue prediction with the SP rule of mixtures technique. The generic integration and equilibrium scheme of the SP-RoM allows different type of constitutive behaviour for each material of the structure. Furthermore, this method is able to account for the transmission of structural effects from one material to the other and the monitoring of the internal stress–strain state on each component material of the volume. At the same time, the

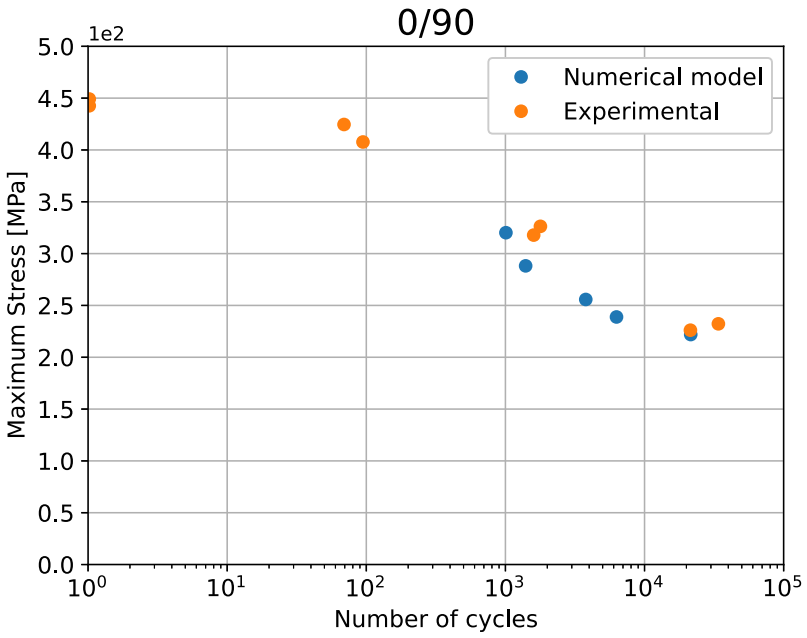


**Fig. 12.** Experimental and numerical data comparison for sequence 0/90.

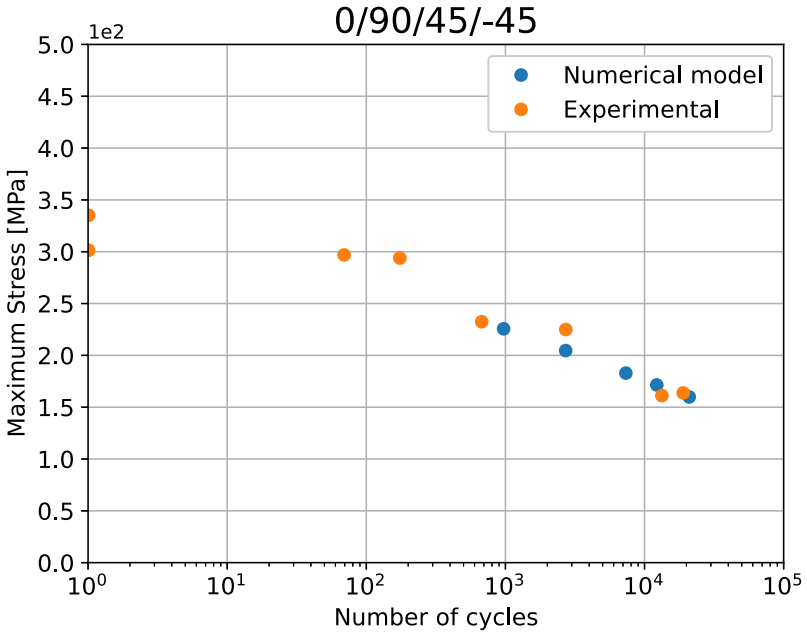


**Fig. 13.** Experimental and numerical data comparison for sequence 0/90/45.

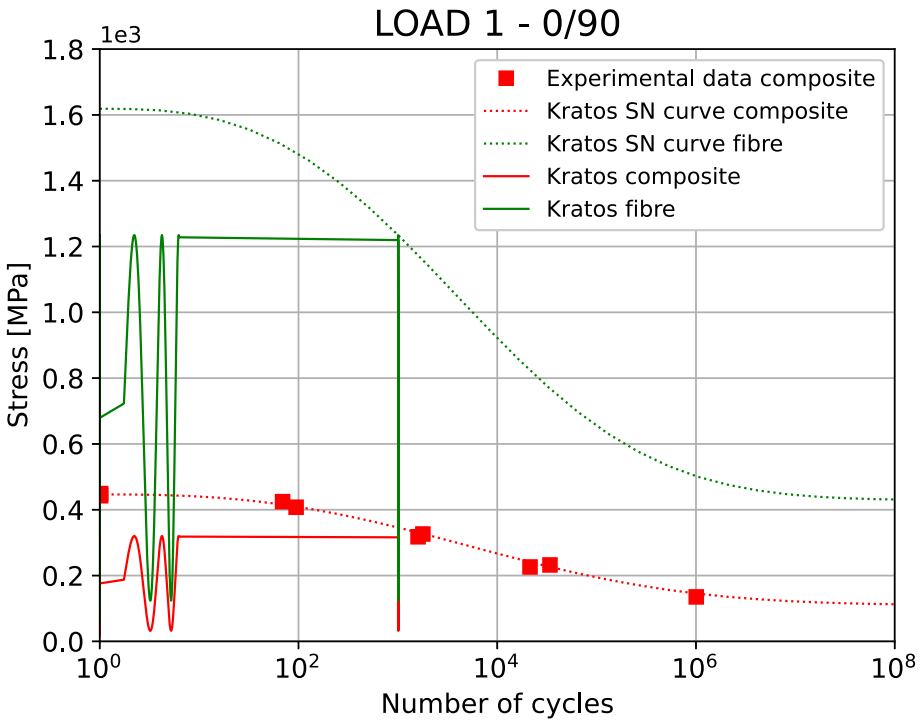


**Fig. 14.** Experimental composite data and fatigue curves of the fibre and both sequences of the composite.

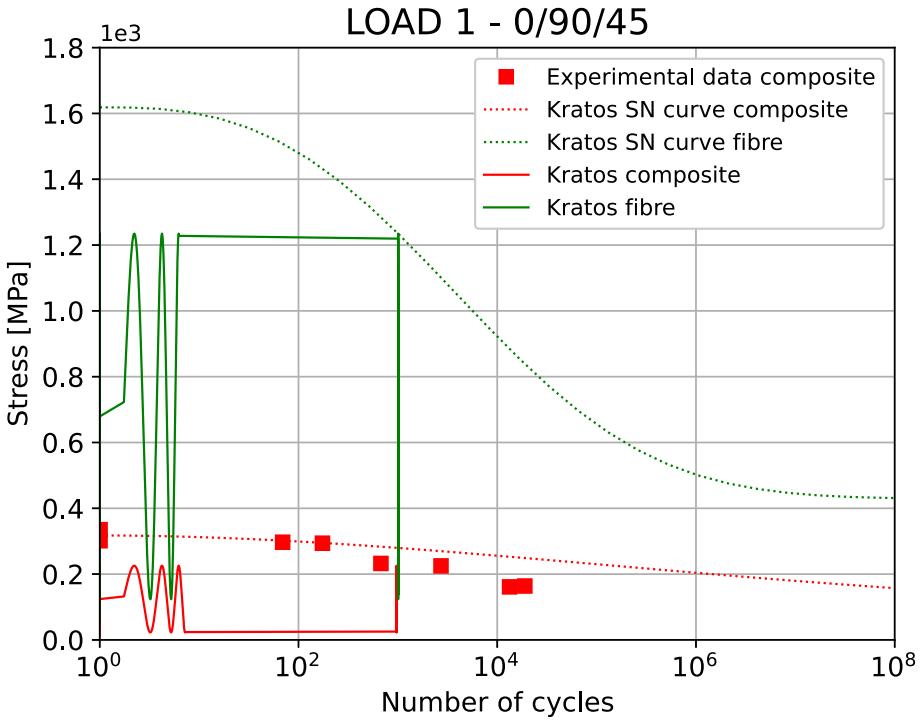


**Fig. 15.** Experimental composite data and fatigue curves of the fibre and both sequences of the composite.

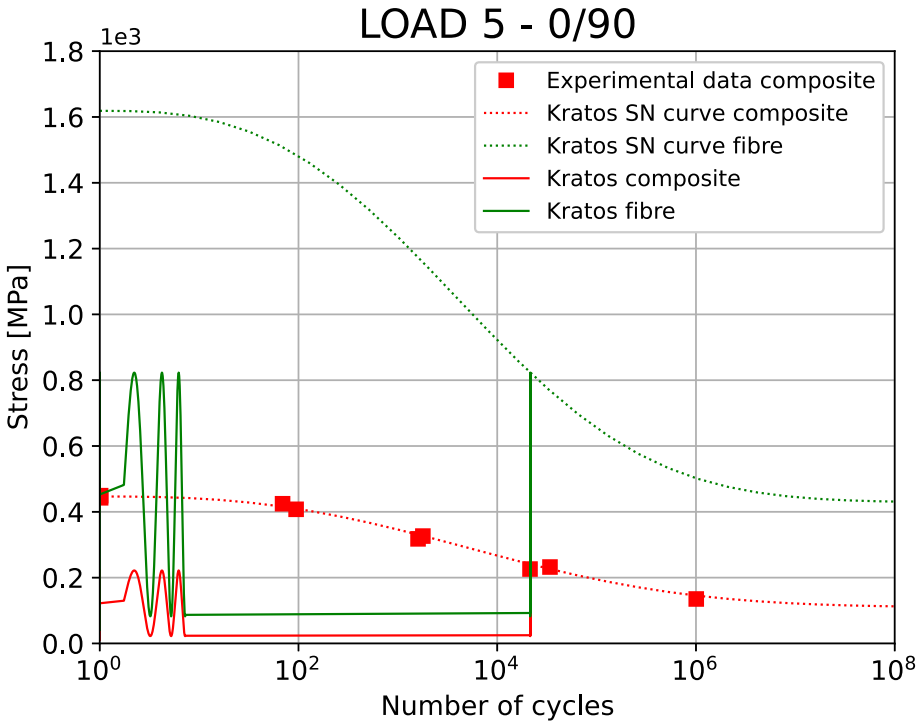


**Fig. 16.** Experimental composite data and fatigue curves of the fibre and the composite.

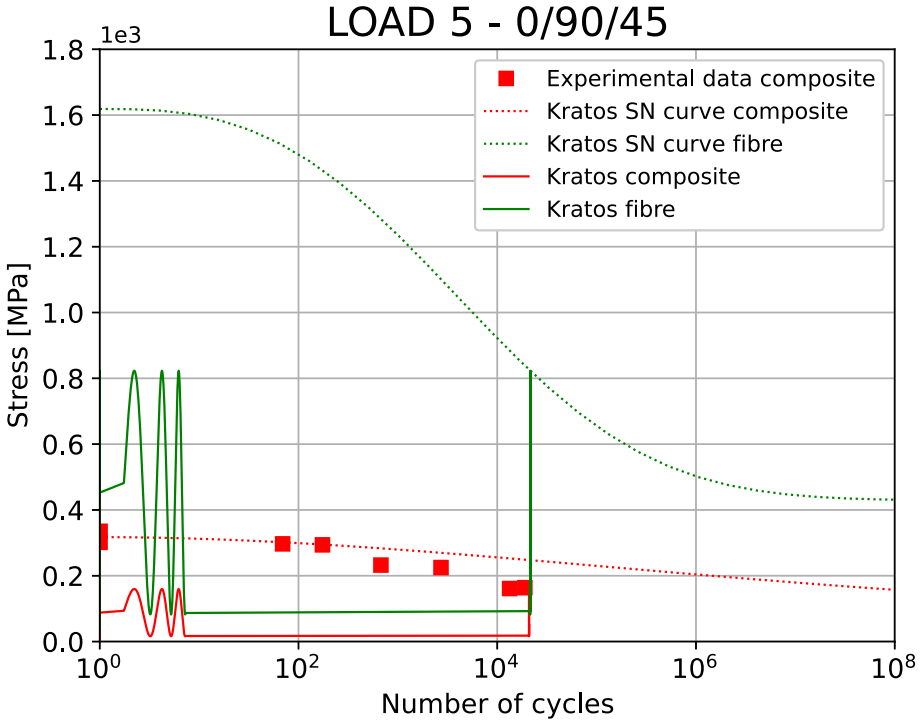


**Fig. 17.** Experimental composite data and fatigue curves of the fibre and the composite.

computational cost is considerably reduced by the use of a cycle jump strategy while still counting with a significant level of information for each material at each integration point of the specimen.

Two cases of two specimens with different stacking sequences have been studied and used as an example of application and validation of the proposed methodology. The fatigue results obtained numerically for the composite material show a high precision in the reproduction of the laboratory tests. On the other hand, it has been checked that the same S–N curve is obtained for different stacking sequences. This validates that the same characterised fibre fatigue parameters can be used for different stacking sequences. Therefore, the most relevant improvement that the proposed methodology offers is the reduction of number of experimental laboratory tests which implies a decrease of time and costs. It is possible to characterised different stacking sequences parting from experimental homogenised data of one stacking sequence. Regarding the time advancing strategy, its correct functioning has been demonstrated showing an accordance between the load applied and the cycle jump.

We can therefore conclude that the formulation is capable of simulating the effect of high cycle fatigue in composite materials. In addition, it allows calibrating the component materials from homogenised data of the composite.

## CRediT authorship contribution statement

**B. Alcayde:** Conceptualization, Formal analysis, Methodology, Software, Validation, Writing – original draft. **M. Merzkirch:** Data curation, Supervision, Writing – review & editing. **A. Cornejo:** Conceptualization, Formal analysis, Investigation, Methodology, Project administration, Software, Supervision, Validation, Writing – original draft, Writing – review & editing. **S. Jiménez:** Methodology, Software, Supervision, Writing – review & editing. **E. Marklund:** Data curation, Investigation. **L.G. Barbu:** Funding acquisition, Project administration, Supervision, Writing – review & editing.

## Data availability

Data will be made available on request.

## Acknowledgements

This work has been done within the framework of the $Fatigue4Light$ project: Fatigue modelling and fast testing methodologies to optimise part design and to boost lightweight materials deployment in chassis parts. This project has received funding from the European Union's Horizon 2020 research and innovation programme under grant agreement No. 101006844. The work has been also supported by the Spanish Government program FPU17/04196 and Severo Ochoa programme through the grant CEX2018-000797-S funded by MCIN/AEI/10.13039/501100011033. The authors Lucia Gratiela Barbu and Alejandro Cornejo are Serra Húnter Fellows. The authors gratefully acknowledge all the received support.

## Declaration of competing interest

The authors declare that they have no known competing financial interests or personal relationships that could have appeared to influence the work reported in this paper.

## Appendix. Time advancing strategy together with the SP-RoM

This appendix includes the structure of the algorithm used to combine the time advancing strategy with the SP-RoM (See Algorithm 1). The stability condition of the cycle is described in 2. The algorithm to actualise the different variables such as the current and the final number of cycles, $N$ and $N_f$, the $ThresholdStress$ and the $MaximumStress$ can be found in Appendix A.2.

**Algorithm 1** Time advancing strategy together with the SP-RoM.

At the end of the time step $t + \Delta t$.
**if** CycleIsFound **then** ▷ Check that the min and max stresses are computed.
  **if** StabilityConditionAchieved **then** ▷ Stability in cycle characteristics. See Alg. 2.
    **if** Damage > 0 in any IP **then**
      Time + = Fixed $\Delta t_{AITS}$ ▷ Fixed amount of time increment. User defined.
    **else**
      **for** Element **do**
        **for** IntegrationPoint **do**
          Compute: $N_f$, $N$, Period, ThresholdStress and MaximumStress ▷ See Alg. 3
          $\Delta t_{AITS,ielem,jIP} = (N_f - N) \cdot CyclePeriod$
        **end for**
      **end for**
      $Time+ = \min \Delta t_{AITS,ielem,jIP}$
    **end if**
  **end if**
**end if**

Notation: $N_f$: Cycles to failure; N: Number of cycles.

### A.1. Cycle stability condition

See Algorithm 2.

**Algorithm 2** Cycle stability condition.

**for** Elements **do** ▷ This loop is done for all the integration points even if the cycle has not changed.
  **if** MaximumStress > ThresholdStress **then**
    $FatigueInCourse = true$
    $AccumulatedMaxStressRelativeError+ = MaximumStressRelativeError$
    $AccumulatedRFactorRelativeError+ = ReversionFactorRelativeError$ ▷ The relative error accounts for the difference in the maximum stress or reversion factor between the current and the previous cycle.
  **end if**
**end for**
**if** (AccumulatedMaxStressRelativeError < $Tol_\sigma$ and AccumulatedRFactorRelativeError < $Tol_R$)
or
(FatigueInCourse and DamageIndicator and AccumulatedMaxStressRelativeError < $Tol_\sigma$ and AccumulatedRFactorRelativeError < $Tol_R$)
**then**
  $AdvancingStrategy = true$
**end if**

Notation: $Tol_\sigma$ and $Tol_R$ are the stress and reversion factor tolerances.

### A.2. Variables calculation at composite level

See Algorithm 3.

**Algorithm 3** Variables calculation at composite level.

Retrieval of a VARIABLE.
**for** NumberOfLayers **do** ▷ We loop over the layers
  **if** Layer is HCF **then** ▷ We check that this layer is HCF CL
    **if** VARIABLE = MaximumStress or VARIABLE = ThresholdStress **then** ▷ We return the layer raw value
      **if** $MaximumStress[Layer] \geq FatigueLimit$ **then** ▷ Check that the stress induces HCF
        $ReturnVARIABLE[Layer]$
      **end if**
    **else if** VARIABLE = VariableRelativeError **then** ▷ Compute the composite relative error of a variable
      $VariableRelativeError += VariableRelativeError[Layer]$ ▷ We accumulate the layer errors and return the sumation
    **else if** VARIABLE = CyclesToFailure **then** ▷ We estimate the time increment at composite level for the AITS
      **if** $MaximumStress[Layer] \geq FatigueLimit$ **then** ▷ Check that the stress induces HCF
        $CyclesToFailure = \min(CyclesToFailure[Layer])$ ▷ We return the most restrictive time increment of the layers
      **end if**
    **else**▷ By default, the composite values are averaged over the layers
      $CompositeVariable+ = VolumetricParticipationLayer \cdot LayerVariable$
    **end if**
  **end if**
**end for**

## References


[1] Sendeckyj George P. Life prediction for resin-matrix composite materials. 1991.

[2] Turon Albert, Costa Josep, Camanho Pedro, Dávila Carlos. Simulation of delamination in composites under high-cycle fatigue. Composites A 2007;38:2270–82. http://dx.doi.org/10.1016/j.compositesa.2006.11.009.

[3] Teimouri Farhad, Heidari-Rarani Mohammad, Haji Aboutalebi Farhad. An XFEM-VCCT coupled approach for modeling mode I fatigue delamination in composite laminates under high cycle loading. Eng Fract Mech 2021;249:107760. http://dx.doi.org/10.1016/j.engfracmech.2021.107760.

[4] Latifi M, Meer FPVan Der, Sluys L. Simulation of delamination growth in laminated composites under high cycle fatigue using a level set model. 2014.

[5] Amiri-Rad Ahmad, Mashayekhi Mohammad, van der Meer Frans P. Cohesive zone and level set method for simulation of high cycle fatigue delamination in composite materials. Compos Struct 2017;160:61–9. http://dx.doi.org/10.1016/j.compstruct.2016.10.041.

[6] Harper Paul, Hallett Stephen. A fatigue degradation law for cohesive interface elements – development and application to composite materials. Int J Fatigue 2010;32:1774–87. http://dx.doi.org/10.1016/j.ijfatigue.2010.04.006.

[7] Bak Brian Lau Verndal, Turón Albert, Lindgaard Esben, Lund Erik. A simulation method for high-cycle fatigue-driven delamination using a cohesive zone model. Internat J Numer Methods Engrg 2016;106:163–91.

[8] Bak BLV, Turon A, Lindgaard E, Lund E. A benchmark study of simulation methods for high-cycle fatigue-driven delamination based on cohesive zone models. Compos Struct 2017;164:198–206. http://dx.doi.org/10.1016/j.compstruct.2016.11.081.

[9] Miehe Christian, Hofacker Martina, Welschinger Fabian. A phase field model for rate-independent crack propagation: Robust algorithmic implementation based on operator splits. Comput Methods Appl Mech Engrg 2010;199:2765–78. http://dx.doi.org/10.1016/j.cma.2010.04.011.

[10] Miehe Christian, Schänzel Lisa-Marie. Phase field modeling of fracture in rubbery polymers. Part I: Finite elasticity coupled with brittle failure. J Mech Phys Solids 2014;65:93–113. http://dx.doi.org/10.1016/j.jmps.2013.06.007.

[11] Loew Pascal, Peters Bernhard, Beex Lars. Fatigue phase-field damage modeling of rubber using viscous dissipation: Crack nucleation and propagation. Mech Mater 2019;142. http://dx.doi.org/10.1016/j.mechmat.2019.103282.

[12] Kuhn Charlotte, Müller Ralf. A continuum phase field model for fracture. Eng Fract Mech 2010;77:3625–34. http://dx.doi.org/10.1016/j.engfracmech.2010.08.009.

[13] Grogan David, Leen Sean, O'Bradaigh Conchur. An XFEM-based methodology for fatigue delamination and permeability of composites. Compos Struct 2014;107:205–18. http://dx.doi.org/10.1016/j.compstruct.2013.07.050.

[14] Bourdin Blaise. Numerical implementation of the variational formulation for quasi-static brittle fracture. Interfaces Free Bound 2007;9:411–30.

[15] Bourdin Blaise, Francfort Gilles, Marigo J-J. The variational approach to fracture. J Elast 2008;91. http://dx.doi.org/10.1007/978-1-4020-6395-4, Reprinted from.

[16] Oller S. Nonlinear dynamics of structures. Barcelona, Spain: Springer; 2014, p. 978–3–319–05193–2.

[17] Oliver Javier, Cervera Miguel, Oller Sergio, Lubliner Jacob. Isotropic damage models and smeared crack analysis of concrete. 2, 1990, p. 945–58.

[18] Barbu Lucia Gratiela. Numerical simulation of fatigue processes: application to steel and composite structures. Universitat Politècnica de Catalunya; 2016.

[19] Ryckelynck D, Missoum Benziane D, Cartel S, Besson J. A robust adaptive model reduction method for damage simulations. Comput Mater Sci 2011;50(5):1597–605. http://dx.doi.org/10.1016/j.commatsci.2010.11.034.

[20] Bhattacharyya Mainak. A model reduction approach in space and time for fatigue damage simulation (Ph.D. thesis), 2018.

[21] Cognard J-Y, Ladevèze P. A large time increment approach for cyclic viscoplasticity. Int J Plast 1993;9(2):141–57. http://dx.doi.org/10.1016/0749-6419(93)90026-M.

[22] Kiefer Konstanze. Simulation of high-cycle fatigue-driven delamination in composites using a cohesive zone model (Ph.D. thesis), Imperial College London; 2014.

[23] Peerlings RHJ, Brekelmans WAM, Borst, de R, Geers MGD. Gradient-enhanced damage modelling of high-cycle fatigue. Internat J Numer Methods Engrg 2000;49(12):1547–69. http://dx.doi.org/10.1002/1097-0207(20001230)49:12<1547::AID-NME16>3.0.CO;2-D.

[24] Kawashita Luiz F, Hallett Stephen R. A crack tip tracking algorithm for cohesive interface element analysis of fatigue delamination propagation in composite materials. Int J Solids Struct 2012;49(21):2898–913. http://dx.doi.org/10.1016/j.ijsolstr.2012.03.034.

[25] Russo Angela, Sellitto Andrea, Curatolo Prisco, Acanfora Valerio, Saputo Salvatore, Riccio Aniello. A robust numerical methodology for fatigue damage evolution simulation in composites. Materials 2021;14(12):3348. http://dx.doi.org/10.3390/ma14123348.

[26] Sally O, Laurin F, Julien C, Desmorat R, Bouillon F. An efficient computational strategy of cycle-jumps dedicated to fatigue of composite structures. Int J Fatigue 2020;135:105500. http://dx.doi.org/10.1016/j.ijfatigue.2020.105500.

[27] Magino Nicola, Köbler Jonathan, Andrä Heiko, Welschinger Fabian, Müller Ralf, Schneider Matti. A space-time upscaling technique for modeling high-cycle fatigue-damage of short-fiber reinforced composites. Compos Sci Technol 2022;222:109340. http://dx.doi.org/10.1016/j.compscitech.2022.109340.

[28] Jiménez Sergio, Barbu Lucia, Oller Sergio, Cornejo Alejandro. On the numerical study of fatigue process in rail heads by means of an isotropic damage based high-cycle fatigue constitutive law. Eng Fail Anal 2021;131:105915. http://dx.doi.org/10.1016/j.engfailanal.2021.105915.

[29] Cornejo A, Barbu LG, Escudero C, Martínez X, Oller S, Barbat AH. Methodology for the analysis of post-tensioned structures using a constitutive serial-parallel rule of mixtures. Compos Struct 2018;200:480–97. http://dx.doi.org/10.1016/j.compstruct.2018.05.123.

[30] Barbu L, Cornejo A, MArtinez X, Oller S, Barbat A. Methodology for the analysis of post-tensioned structures using a constitutive serial-parallel rule of mixtures: Large scale non-linear analysis. Compos Struct 2019;216.

[31] Jimenez S, Cornejo A, Barbu LG, Oller S, Barbat AH. Analysis of the mock-up of a reactor containment building: comparison with experimental results. Nucl Eng Des 2020;359:110454.

[32] Jiménez S, Cornejo A, Barbu LG, Barbat AH, Oller S. Failure pressure analysis of a nuclear reactor prestressed concrete containment building. Eng Struct 2021;236:112052. http://dx.doi.org/10.1016/j.engstruct.2021.112052.

[33] Cornejo A, Mataix V, Wriggers P, Barbu LG, Oñate E. A numerical framework for modelling tire mechanics accounting for composite materials, large strains and frictional contact. Comput Mech 2023. http://dx.doi.org/10.1007/s00466-023-02353-4.

[34] Ansari Md Touhid Alam, Singh Kalyan Kumar, Azam Mohammad Sikandar. Fatigue damage analysis of fiber-reinforced polymer composites—A review. J Reinf Plast Compos 2018;37(9):636–54.

[35] Adam TJ, Horst P. Fatigue damage and fatigue limits of a GFRP angle-ply laminate tested under very high cycle fatigue loading. Int J Fatigue 2017;99:202–14.

[36] Colombo Chiara, Libonati Flavia, Vergani LAURA. Fatigue damage in GFRP. Int J Struct Integr 2012.

[37] Knoll Julia B, Koschichow Roman, Koch Ilja, Schulte Karl, Gude Maik. Failure mode specific fatigue testing of nanoparticle-modified cfrp under vhcf-loading. In: CompTest 2013-book of abstracts. 2013, p. 99.

[38] Cornejo Alejandro, Oñate Eugenio, Zarate Francisco. A fully Lagrangian formulation for fluid-structure interaction between free-surface flows and multi-fracturing solids (Ph.D. thesis), 2020.

[39] de Spuza E, Peric D, Owen RJ. Computational methods for plasticity: Theory and applications. Wiley; 2008.

[40] Oller Sergio, Salomón Omar, Oñate Eugenio. A continuum mechanics model for mechanical fatigue analysis. Comput Mater Sci 2005;32(2):175–95. http://dx.doi.org/10.1016/j.commatsci.2004.08.001.
[41] Ferrándiz VM, Bucher P, Rossi R, Cotela J, et al. KratosMultiphysics (Version 8.1). Zenodo; 2020.
[42] Oller S, Barbat AH, Onate E, Hanganu A. A damage model for the seismic analysis of building structures. In: Congreso Mundial de Ingeniería Antisísmica. 1992.
[43] Rastellini F, Oller S, Salomon O, Oñate E. Composite materials non-linear modelling for long fibre-reinforced laminates: Continuum basis, computational aspects and validations. Comput Struct 2008;86(9):879–96, Composites.
[44] Rastellini F. Modelización numérica de la no-linealidad constitutiva de laminados compuestos (Ph.D. thesis), Departament de Resistència de Materials i Estructures a l'Enginyeria (RMEE) - UPC, 2006. Directors, Sergio Oller and Eugenio Oñate; 2006.
[45] Car E. Modelo constitutivo continuo para el estudio del comportamiento mecánico de los materiales compuestos (Ph.D. thesis), Departament de Resistència de Materials i Estructures al'Enginyeria (RMEE) - UPC, 2000. Directors, Sergio Oller and Eugenio Oñate; 2000.
[46] Merzkirch M, Tabib P. Structural analysis and modeling of GFRP and FML under fatigue loading conditions. Int J Fatigue 2024.
[47] Dadvand Pooyan, Rossi Riccardo, Oñate Eugenio. An object-oriented environment for developing finite element codes for multi-disciplinary applications. Arch Comput Methods Eng 2010;17:253–97.